



HAL
open science

Cone-beam reconstruction for a circular trajectory with transversely-truncated projections based on the virtual fan-beam method

Mathurin Charles, Rolf Clackdoyle, Simon Rit

► **To cite this version:**

Mathurin Charles, Rolf Clackdoyle, Simon Rit. Cone-beam reconstruction for a circular trajectory with transversely-truncated projections based on the virtual fan-beam method. 7th International Conference on Image Formation in X-Ray Computed Tomography 2022, Jun 2022, Baltimore, United States. pp.38, 10.1117/12.2646482 . hal-03821853

HAL Id: hal-03821853

<https://hal.science/hal-03821853>

Submitted on 19 Oct 2022

HAL is a multi-disciplinary open access archive for the deposit and dissemination of scientific research documents, whether they are published or not. The documents may come from teaching and research institutions in France or abroad, or from public or private research centers.

L'archive ouverte pluridisciplinaire **HAL**, est destinée au dépôt et à la diffusion de documents scientifiques de niveau recherche, publiés ou non, émanant des établissements d'enseignement et de recherche français ou étrangers, des laboratoires publics ou privés.

Cone-beam reconstruction for a circular trajectory with transversely-truncated projections based on the virtual fan-beam method

Mathurin Charles^a, Rolf Clackdoyle^b, and Simon Rit^c

^{a,b}Univ. Grenoble Alpes, CNRS, TIMC UMR 5525, Grenoble, France

^cUniv. de Lyon, INSA-Lyon, Univ. Claude Bernard Lyon 1, UJM-Saint Etienne, CNRS, INSERM, CREATIS UMR 5220, U1294, F-69373, Lyon, France

ABSTRACT

We describe a new procedure for three-dimensional (3D) region-of-interest (ROI) reconstruction from transversely-truncated cone-beam projections acquired with a circular source trajectory. This method is an extension to 3D of the virtual fan-beam (VFB) method. It is based on a VFB formula that performs the backprojection in the acquisition geometry. Our simulation results show that the ROI reconstruction of the 3D Shepp-Logan phantom is very similar to the one obtained by the Feldkamp, Davis, Kress (FDK) algorithm without truncation. However the reconstruction of the Forbild head phantom shows artefacts which are absent from the FDK truncation-free reconstruction.

1. INTRODUCTION

In three-dimensional (3D) cone-beam computed tomography (CBCT), a common source trajectory is a circular scanning around the object. The plane containing the circular source trajectory is usually called the central plane, midplane or source plane. From Tuy's data sufficiency condition,¹ we know that mathematically exact reconstruction of the object density is possible only in the midplane. In case of non-truncated cone-beam projections, the well-known and widely used Feldkamp-Davis-Kress (FDK) algorithm² provides exact reconstruction in the central plane and approximate reconstruction elsewhere. This algorithm, which can be seen as a heuristic extension of the fan-beam filtered backprojection (FBP) formula for two-dimensional (2D) reconstruction, applies a ramp filter to each projection row. Consequently, the FDK formula is not suitable for treating transversely-truncated cone-beam projections.

We distinguish two kinds of situations with transverse truncation. In the first one, the detector is placed off-center so that, even if the detector does not cover the object laterally, each ray-line in the midplane is measured at least once during a 360° scan. It is thus possible, in the midplane, to obtain the missing information of a truncated projection from other projections. Elsewhere, the same procedure is applied to all the other rows of the projections even though the missing rays and measured rays have a different angle with the central plane. Using this idea, several methods have been proposed such as a pre-convolution weighting of the projections before applying the FDK³ and a 3D version of a Katsevich-type FBP.⁴

The second kind of situation with truncated cone-beam projections is when the detector, which still does not cover the whole object, is centered (when a ray-line passing through the center of rotation of the source hits the center of the detector). In that case, we define the measured area as the region imaged by every source position, and it corresponds to the volume inside a cylinder which does not contain the whole object. Considering a full scan acquisition trajectory, it follows that, in the midplane, every line passing through this area is measured. So we call field-of-view (FOV) the midplane slice of the measured area. In this situation, it is not possible to obtain missing line-integrals in the midplane from other source positions so the previous methods cannot be applied. However, there are two analytical methods which can perform region-of-interest (ROI) reconstruction from truncated projections in the midplane: the differentiated back-projection (DBP)^{5,6} method, also called back-projection filtration (BPF);⁷ and the virtual fan-beam (VFB) method.⁸ The BPF has been extended to

Send correspondence to M.C.: mathurin.charles@univ-grenoble-alpes.fr

three dimensions⁹ but, to our knowledge, not the VFB method. In this work, we propose to extend the VFB method to 3D ROI reconstruction in the case of transversely-truncated cone-beam projections acquired with a circular source trajectory.

In the usual 2D context, the principle of the VFB method is to identify a virtual source trajectory for which we have non-truncated projections and to rebin the truncated projections into this geometry. Then, super-short-scan formulas¹⁰ can be used to perform the reconstruction. To choose the virtual trajectory, we use the fact that acquired data can be rebinned into non-truncated projections for any point inside the FOV and outside the convex hull, as we have access to the integral of any half-line extending from this point. In a previous contribution, we proposed a VFB formula¹¹ for a circular fan-beam acquisition geometry, for which the backprojection was performed in the acquisition geometry. In this work, we extend this approach to 3D.

2. THEORY

2.1 Notation

Let $\vec{\theta}_\lambda = (\cos \lambda, \sin \lambda, 0)$, $\vec{\eta}_\lambda = (-\sin \lambda, \cos \lambda, 0)$ and $\vec{e}_z = (0, 0, 1)$ (in 2D, the last component of $\vec{\theta}_\lambda$ and $\vec{\eta}_\lambda$ is discarded). Let f denote the 3D object density to be reconstructed. The cone-beam projections of f for a circular source trajectory of radius R_A acquired on a flat detector placed at the origin O are defined by

$$\bar{g}^{RA}(\lambda, u, v) = \int_0^{+\infty} f \left(R_A \vec{\theta}_\lambda + l \frac{-R_A \vec{\theta}_\lambda - u \vec{\eta}_\lambda + v \vec{e}_z}{\sqrt{R_A^2 + u^2 + v^2}} \right) dl \quad (1)$$

where $\lambda \in \Lambda = [0, 2\pi)$ and $S(\Lambda) = R_A \vec{\theta}_\Lambda$ is the set of vertices (cone-beam source locations) of the trajectory (see figure 1).

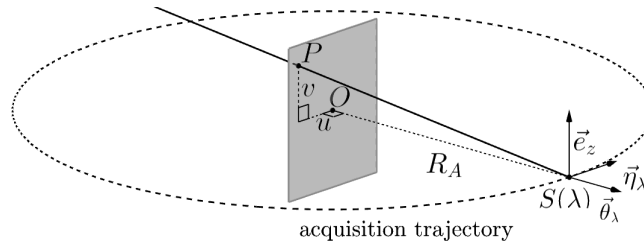


Figure 1. The circular acquisition geometry of center O and radius R_A . The point $S(\lambda)$ is a vertex of the trajectory. A ray passing through the point P on the detector placed at the origin O is identified by the parameters (λ, u, v) .

In 2D, the fan-beam projections of f for a circular source trajectory of radius R_A with angular parametrization are defined by

$$g^{RA}(\lambda, \gamma) = \int_0^\infty f(R_A \vec{\theta}_\lambda - t \vec{\theta}_{\lambda+\gamma}) dt \quad (2)$$

where $\gamma \in (-\pi/2, \pi/2)$ is the usual ray-angle measured counterclockwise with respect to the central ray (which is defined by the source and the center of rotation). The parameters u and γ (respectively for equispaced rays and equiangular rays) are linked by $u = R_A \tan \gamma$ so, in the midplane, we have

$$g^{RA}(\lambda, \gamma) = \bar{g}^{RA}(\lambda, R_A \tan \gamma, 0) \text{ and } \bar{g}^{RA}(\lambda, u, 0) = g^{RA}(\lambda, \arctan(u/R_A)). \quad (3)$$

2.2 Configuration studied

We consider the following configuration. The measured area is the volume inside a cylinder of center O , extended axially without limit since we consider no axial truncation. We assume that the support of the object function is contained within a known ellipsoid which extends outside the measured area (see figure 2 left).

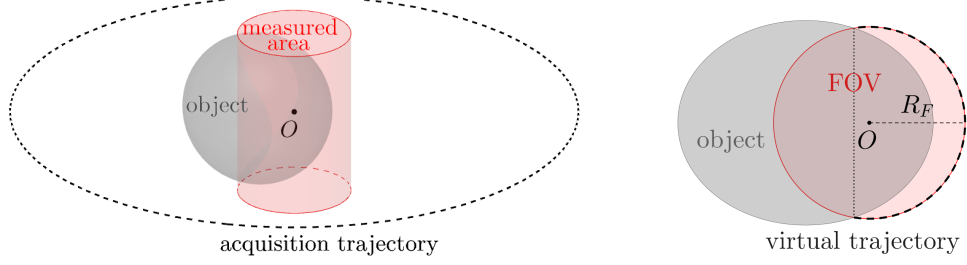


Figure 2. Left: the ellipsoid object is partially covered by the cylindrical measured area (drawn in red). Right: situation in the midplane. The circular FOV of center O and radius R_F covers only a part of the elliptic object. The virtual trajectory is the black arc of circle of center O and radius $R_V = R_F$ and the vertical black dashed line is the boundary of its convex hull.

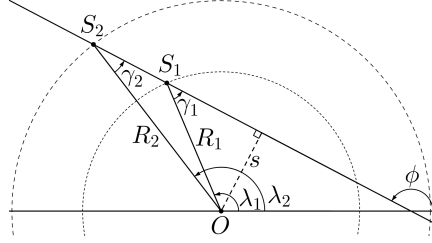


Figure 3. The parameters (λ_i, γ_i) of a ray for source trajectories of radius R_i with $i \in \{1, 2\}$ are linked through $s = R_i \sin \gamma_i$ and $\phi = \lambda_i + \gamma_i$.

2.3 The VFB formula used in the midplane

In the midplane, the 2D slice of the object has an elliptic support and the FOV has a circular support. The chosen virtual trajectory is the arc of circle at the border of the FOV and outside the object (see figure 2 right). In that case, the area for which the VFB method is mathematically exact is the convex hull of the virtual trajectory.

We now recall our VFB formula from.¹¹ The rebinning relations between two trajectories with different radius can be seen on figure 3. The data are first rebinned from the acquisition geometry of radius R_A to the virtual geometry of radius R_V using

$$g^{R_V}(\lambda, \gamma) = g^{R_A}(\lambda + \gamma - \gamma_{R_A}^{R_V}, \gamma_{R_A}^{R_V}) \quad (4)$$

where

$$\gamma_{R_A}^{R_V} = \arcsin\left(\frac{R_V}{R_A} \sin \gamma\right). \quad (5)$$

Then, differentiation and Hilbert filtering is performed on the non-truncated projections in the virtual geometry with

$$g_F^{R_V}(\lambda, \gamma) = \frac{1}{2\pi} \int_{-\pi}^{\pi} h_H(\sin(\gamma - \gamma'))(\partial_1 - \partial_2)g^{R_V}(\lambda, \gamma')d\gamma'. \quad (6)$$

where $h_H(s) = \int_{\mathbb{R}} -i \operatorname{sign}(\sigma)e^{2i\pi\sigma s}d\sigma$ denotes the Hilbert filter and ∂_i corresponds to the partial derivative with respect to the i -th variable. As the virtual trajectory is not a full scan, the redundancy in the filtered projections is handled by applying a weight w^{R_V} (that we do not detail) to $g_F^{R_V}$: $\tilde{g}_F^{R_V}(\lambda, \gamma) = w^{R_V}(\lambda, \gamma) g_F^{R_V}(\lambda, \gamma)$. Next, the filtered projections in the acquisition geometry are obtained from the filtered projections in the virtual geometry by

$$g_F^{R_A}(\lambda, \gamma) = \frac{R_A \cos \gamma}{\sqrt{R_V^2 - R_A^2 \sin^2 \gamma}} \tilde{g}_F^{R_V}(\lambda + \gamma - \gamma_{R_V}^{R_A}, \gamma_{R_V}^{R_A}) \quad (7)$$

where

$$\gamma_{R_V}^{R_A} = \arcsin\left(\frac{R_A}{R_V} \sin \gamma\right). \quad (8)$$

Finally, the backprojection is performed in the acquisition geometry. For every \vec{x} in the convex hull of the virtual trajectory, we have:

$$f(\vec{x}) = - \int_0^{2\pi} \frac{1}{\|R_A \vec{\theta}_\lambda - \vec{x}\|} g_F^{R_A}(\lambda, \gamma_{\vec{x}, \lambda}) d\lambda \quad (9)$$

where

$$\gamma_{\vec{x}, \lambda} = \arctan \left(\frac{-\vec{x} \cdot \vec{\eta}_\lambda}{R_A - \vec{x} \cdot \vec{\theta}_\lambda} \right). \quad (10)$$

We can see that this formula is designed for equiangular data $g^{R_A}(\lambda, \gamma)$. As we consider equispaced data $\bar{g}^{R_A}(\lambda, u, v)$ in this paper, an additional rebinning using equation (3) left is required before using the VFB formula above.

2.4 Modifying the VFB method for cone-beam projections

We now detail how the VFB formula above is modified to be used on cone-beam projections. First, we perform a weighting of the cone-beam projections:

$$\bar{g}_W^{R_A}(\lambda, u, v) = \bar{g}^{R_A}(\lambda, u, v) \frac{\sqrt{R_A^2 + u^2}}{\sqrt{R_A^2 + u^2 + v^2}} \quad (11)$$

For an object that is constant in z , (11) ensures that for all v : $\bar{g}_W^{R_A}(\lambda, u, v) = \bar{g}_W^{R_A}(\lambda, u, 0)$, so the exact reconstruction area will be extended axially if each row of the weighted projections is treated as the row in the midplane.

Then, for all the weighted data rows $\bar{g}_W^{R_A}(\lambda, u, v)$ of parameter v fixed, we perform the following steps as if the transaxial plane of height $z = v$ was the source plane, using the same virtual source trajectory as in the midplane:

1. Rebinning of the data rows to the virtual geometry:

$$\bar{g}^{R_V}(\lambda, \gamma, v) = \bar{g}_W^{R_A}(\lambda + \gamma - \gamma_{R_A}^{R_V}, R_A \tan \gamma_{R_A}^{R_V}, v) \quad (12)$$

2. Differentiation and Hilbert-filtering of the virtual data:

$$\bar{g}_F^{R_V}(\lambda, \gamma, v) = \frac{1}{2\pi} \int_{-\pi}^{\pi} h_H(\sin(\gamma - \gamma')) (\partial_1 - \partial_2) \bar{g}^{R_V}(\lambda, \gamma', v) d\gamma' \quad (13)$$

3. Rebinning to acquisition geometry with weighting w^{R_V} :

$$\bar{g}_F^{R_A}(\lambda, u, v) = \frac{R_A \cos \gamma}{\sqrt{R_V^2 - R_A^2 \sin^2 \gamma}} (\bar{w}^{R_V} \bar{g}_F^{R_V})(\lambda + \gamma - \gamma_{R_V}^{R_A}, \gamma_{R_V}^{R_A}, v) \quad (14)$$

where we take $\bar{w}^{R_V}(\lambda, \gamma, v) = w^{R_V}(\lambda, \gamma)$ for all v , and $\gamma = \arctan(u/R_A)$.

Finally, the backprojection is performed in the acquisition geometry to give \hat{f} , the 3D VFB reconstruction :

$$\hat{f}(\vec{x}, z) = - \int_0^{2\pi} \frac{1}{\|R_A \vec{\theta}_\lambda - \vec{x}\|} \bar{g}_F^{R_A}(\lambda, u_{\vec{x}, \lambda}, v_{\vec{x}, z, \lambda}) d\lambda \quad (15)$$

for \vec{x} in the convex hull of the virtual source trajectory,

$$u_{\vec{x}, \lambda} = \frac{-R_A \vec{x} \cdot \vec{\eta}_\lambda}{R_A - \vec{x} \cdot \vec{\theta}_\lambda} \quad \text{and} \quad v_{\vec{x}, z, \lambda} = \frac{R_A z}{R_A - \vec{x} \cdot \vec{\theta}_\lambda}. \quad (16)$$

3. EXPERIMENTS AND RESULTS

3.1 Simulations

The simulations were performed on a 3D version of the Shepp-Logan phantom and on the 3D head Forbild phantom*. The reconstructed image was computed on a cubic grid of size $[401, 401, 401]$ voxels. The data were acquired on a circular trajectory of center $O = (0, 0, 0)$ and radius R_A , using the software RTK.¹² The projections were transversely truncated such that the measured area was a cylinder of center O and radius R_F . The virtual source trajectory radius was $R_V = R_F$. The acquisition trajectory along $[0, 2\pi)$ was sampled with N_λ vertices and each projection was composed of $N_u \times N_v$ ray-lines. The virtual trajectory was composed of $N_{\lambda_{\text{virt}}}$ virtual segments and each virtual projection was composed of $N_{\gamma_{\text{virt}}}$ ray-lines. For the Shepp-Logan phantom, we took $R_A = 4$, $R_F = 0.8$, $N_\lambda = 1256$, $N_u = 409$, $N_v = 517$, $N_{\lambda_{\text{virt}}} = 879$ and $N_{\gamma_{\text{virt}}} = 1257$. For the head Forbild phantom, we took $R_A = 45$, $R_F = 9$, $N_\lambda = 1256$, $N_u = 409$, $N_v = 603$, $N_{\lambda_{\text{virt}}} = 693$ and $N_{\gamma_{\text{virt}}} = 1257$.

3.2 Results

Figure 4 shows, for three slices of the 3D Shepp-Logan phantom (left) and the head Forbild phantom (right), the reference image, the reconstructed image using the FDK algorithm with non-truncated data, the reconstructed image using our modified 3D VFB method for transversely-truncated data, and the profiles of the lines drawn in white on the reference and the 3D VFB reconstructions. The mathematically exact reconstruction area (convex hull of the virtual source trajectory), which we also call the recoverable area, is delimited by a black dashed line on the 3D VFB reconstructions.

Looking at figure 4 left, we can see that the 3D VFB reconstruction is excellent in the recoverable area in the midplane (left column). In the planes at $x = 0$ (middle column) and at $y = 0.4$ (right column), the reconstruction is still very good when we are close to the midplane. Further away from the midplane, we observe a slow decrease of the intensity when $|z|$ increases, similar to that on the FDK reconstruction, although not exactly the same. There are also slight horizontal streak artefacts, tangent to the white ellipse, which are less marked on the FDK reconstruction.

The 3D VFB reconstruction of the Forbild head phantom (figure 4 right) is good in the recoverable area in the midplane (left column), but far less accurate than what we obtained for the Shepp-Logan phantom in figure 4 left. The difference is that the Forbild phantom consists of many more and finer anatomical structures than the Shepp-Logan phantom, making it a far more challenging phantom to reconstruct. Consequently, we observe that the FDK and 3D VFB reconstructions suffer from many artefacts for planes at $x = 0$ (middle column) and at $y = -1$ (right column). The artefacts are stronger for the 3D VFB reconstruction, as we observe for instance with the white area at the right of the black ellipse at plane $x = 0$ (middle column), and also with the large black horizontal streak covering the top of the two circular structures at plane $y = -1$ (right column).

4. CONCLUSION

In this work, we proposed a 3D version of the VFB method, based on a VFB formula performing the backprojection in the circular acquisition geometry and detailed in a previous contribution.¹¹ This method was used for ROI reconstruction from transversely-truncated cone-beam projections acquired with a circular source trajectory. The numerical results were accurate in the midplane but only approximate outside the midplane. For the Forbild head phantom especially, strong artefacts appeared in the 3D VFB reconstruction that were absent from the FDK truncation-free reconstruction. Both the FDK algorithm and the 3D VFB had to address the incompleteness of a circular cone-beam trajectory, but the 3D VFB was also handling truncated data, so it was not surprising that different artefacts appeared in the off-plane reconstructed images.

ACKNOWLEDGMENTS

This work was supported by grants ANR-17-CE19-0006 (ROIdoré) and ANR-21-CE45-0026 (SPECT-Motion-eDCC) from the Agence Nationale de la Recherche, France.

*See <http://www.imp.uni-erlangen.de/phantoms/head/head.html>.

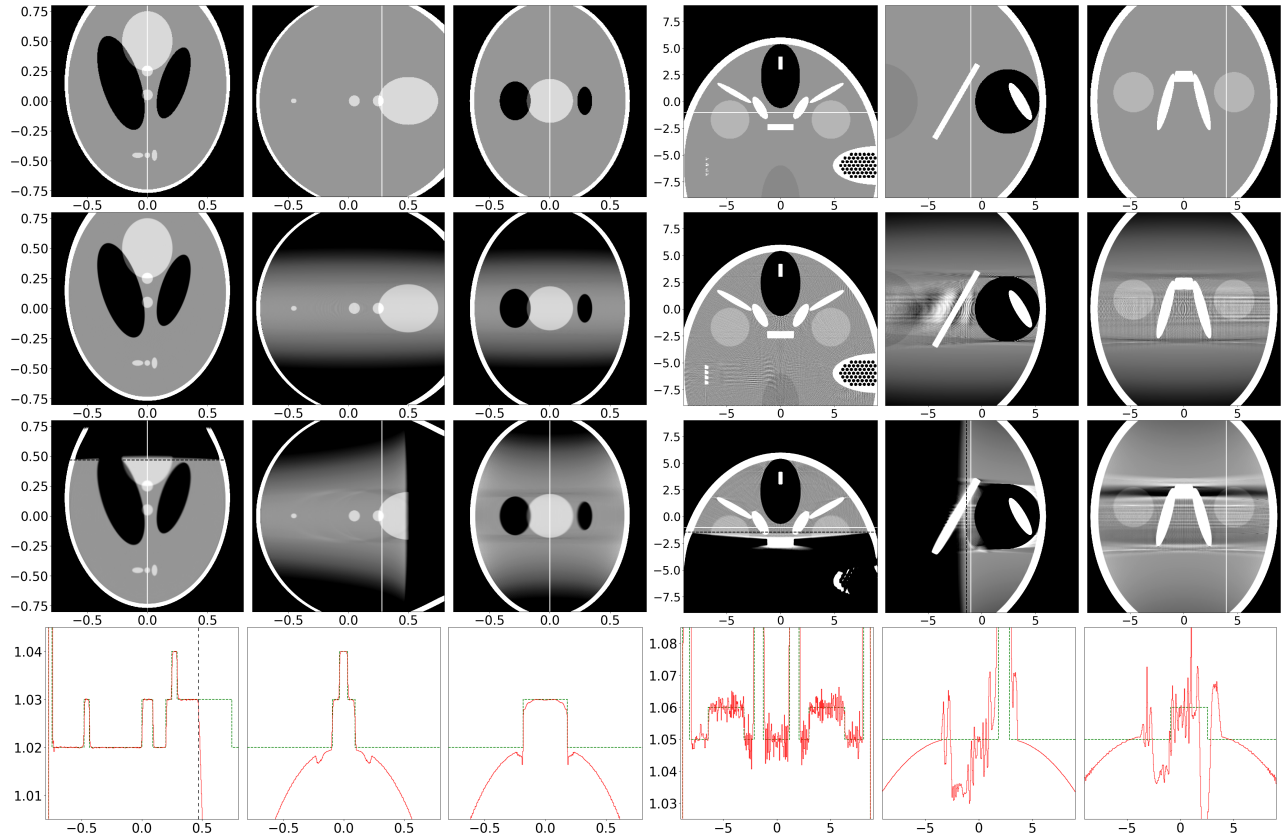


Figure 4. Left block: 3D Shepp-Logan (SL) phantom. Right block: Forbild head phantom. For each block: Left column: (x, y) plane at $z = 0$. Middle column: (y, z) plane at $x = 0$. Right column: (x, z) plane at $y = 0.4$. Top row: 2D slices of the reference phantom. Middle row 1: reconstruction using the FDK algorithm without truncation. Middle row 2: reconstruction using our 3D VFB algorithm with truncation. The black dashed line defines the boundary of the possible reconstruction area. The plotting scale is respectively [1.0 (black), 1.04 (white)] for the SL phantom and [1.0 (black), 1.1 (white)] for the head phantom. Bottom row: profile corresponding to the white line, plotted with scale [1.005, 1.045] for the for the SL phantom and with scale [1.025, 1.085] for the head phantom. The reference profile is plotted in green dashed line and the real one in red.

REFERENCES

- [1] Tuy, H. K., “An Inversion Formula for Cone-Beam Reconstruction,” *SIAM J. Appl. Math.* **43**(3), 546–552 (1983).
- [2] Feldkamp, L. A., Davis, L. C., and Kress, J. W., “Practical cone-beam algorithm,” *J. Opt. Soc. Amer. A* **1**(6), 612 (1984).
- [3] Cho, P. S., Rudd, A. D., and Johnson, R. H., “Cone-beam CT from width-truncated projections,” *Comput. Med. Imag. Graph.* **20**(1), 49–57 (1996).
- [4] Schäfer, D., Grass, M., and van de Haar, P., “FBP and BPF reconstruction methods for circular X-ray tomography with off-center detector,” *Med. Phys.* **38**(S1), S85–S94 (2011).
- [5] Noo, F., Clackdoyle, R., and Pack, J. D., “A two-step Hilbert transform method for 2D image reconstruction,” *Phys. Med. Biol.* **49**(17), 3903–3923 (2004).
- [6] Zhuang, T., Leng, S., Nett, B. E., and Chen, G., “Fan-beam and cone-beam image reconstruction via filtering the backprojection image of differ-entiated projection data,” *Phys. Med. Biol.* **49**(24), 5489–5503 (2004).
- [7] Zou, Y., Pan, X., and Sidky, E. Y., “Image reconstruction in regions-of-interest from truncated projections in a reduced fan-beam scan,” *Phys. Med. Biol.* **50**(1), 13–27 (2004).

- [8] Clackdoyle, R., Noo, F., Guo, J., and Roberts, J. A., “Quantitative reconstruction from truncated projections in classical tomography,” *IEEE Trans. Nucl. Sci.* **51**(5), 2570–2578 (2004).
- [9] Yu, L., Zou, Y., Sidky, E. Y., Pelizzari, C. A., Munro, P., and Pan, X., “Region of interest reconstruction from truncated data in circular cone-beam CT,” *IEEE Trans. Med. Imag.* **25**(7), 869–881 (2006).
- [10] Noo, F., Defrise, M., Clackdoyle, R., and Kudo, H., “Image reconstruction from fan-beam projections on less than a short scan,” *Phys. Med. Biol.* **47**(14), 2525–2546 (2002).
- [11] Charles, M., Clackdoyle, R., and Rit, S., “Implementation of the virtual fan-beam method for 2D region-of-interest reconstruction from truncated data,” in [*Fully 3D Image Recon. Radiol. Nucl. Med.*], 44–48 (2021).
- [12] Rit, S., Oliva, M. V., Brousmiche, S., Labarbe, R., Sarrut, D., and Sharp, G. C., “The Reconstruction Toolkit (RTK), an open-source cone-beam CT reconstruction toolkit based on the Insight Toolkit (ITK),” *Journal of Physics: Conference Series* **489**, 012079 (2014).